X International Conference on Computational Methods in Marine Engineering
MARINE 2023
J. Garcia-Espinosa, L. González, J.E. Gutiérrez & B. Serván-Camas (Editors)

Numerical investigation on the characteristics of Two-phase flow field of inclined pipes with vibration based on MPS-DEM method

MARINE 2023

Renxiang Li[1], Fengze Xie[2], Decheng Wan[3]*

[1] Computational Marine Hydrodynamics Lab (CMHL), Shanghai Jiao Tong University, Campus Minhang, Shanghai 200240 China. E-mail: l18041106760@163.com

* Corresponding author: Decheng Wan, dcwan@sjtu.edu.cn

ABSTRACT

Deep-sea mining uses risers for mineral transport. However, the pipeline may incline and vibrate due to the wind and current (Avi, 2018). Study on the influence of pipe vibration types on the internal flow field characteristics is significant. Considering the two-phase flow in the pipeline and the turbulence caused by vibration, in this paper, a numerical method coupled with moving particle semi-implicit method (MPS) and discrete element method (DEM) is adopted, this method has advantages in dealing with violent flow problem. The MPSDEM-SJTU solver independently developed by the CMHL is used to simulate pipes with different vibration direction. According to results of numerical simulation, the pipeline pressure loss fluctuates with time. In addition, the influence of vibration direction on flow field characteristics such as fluid velocity, solid particle volume fraction and particles flow state are also analyzed. The results of numerical simulation can provide a reference for the optimization of hydraulic lifting system.

Keywords: MPS method, DEM method, Two-phase flow, Pipelines, Vibration.

NOMENCLATURE

ε_p	local volume fraction
$\vec{u}$	Velocity vector [m/s]
μ_p	Aerodynamic force vector [Pa·s]
$\vec{p}_{int}$	Volume force [N]
r_e	Radius of the particle's scope[m]
I_p	Moment of inertia [kg·m²]
ω_p	Angular velocity [rad]
F_p^{int}	Hydrodynamic vector [N]
F_p^d	Drag force [N]
V_p	Volume of solid particles [m^3]
v_p	Velocity of solid particles [m/s]
β_p	Interface momentum exchange coefficient

MPS	Moving Particle Semi-implicit Method
DEM	Discrete Element Method

1. INTRODUCTION

In recent years, with the advancement of deep-sea mining, long-distance pipelines have been widely used for mineral transportation, and the problem of solid-liquid two-phase transportation has become a research hotspot (Oh *et al.*, 2015). During deep-sea mining, pipelines may tilt and vibrate due to the combined influence of wind, waves, and currents. Unlike the static pipeline transport on land, it is obvious that the inclination and vibration of the pipeline make the flow field characteristics inside the pipeline change, and the study of the flow filed change is of great significance for improving the hydraulic lifting system.

The transportation process inside pipelines is complex and variable, making the study difficult. Hashemi *et al.* (2016) used the experimental method to summarize the empirical rules, but the repeatability of this method is low, and the economic cost is high. In addition, when applied to the working condition of high Reynolds number like vibrating pipes, the results are difficult to conform to the real situation. Therefore, numerical simulation methods have emerged, but for vibrating pipelines, the application of numerical simulation methods is very difficult. Especially in the selection of interaction models between solid particles and liquid, and there is a contradiction between the accuracy of numerical simulation and the computational complexity.

Numerical simulation methods can be mainly divided into two types: Euler method and Lagrangian method. The Euler-Euler method (Messa and Malavasi, 2015) uses the Euler method for both solid and liquid phases, which requires less computation but cannot accurately calculate the motion details of particles. The Euler-Lagrangian method (Jafari *et al*., 2014) can ensure the accuracy of solving solid particles, but it has high requirements for grids. The Lagrangian-Lagrangian method uses the Lagrangian method for both solid and liquid phases. This type of method can accurately describe the collision process between particles, mainly including two coupling methods: SPH-DEM (Martin *et al*., 2014) and MPS-DEM (Li *et al*., 2019). At present, many scholars have adopted the above methods to study the two-phase flow problems. Messa *et al*. (2014) used the dual fluid method to simulate the hydraulic transportation of mud and successfully predicted the pressure drop and concentration distribution, but this method failed to simulate the friction stress which plays an important role in the transportation process. Avi *et al*. (2018) used the CFD-DEM method to simulate the particle transport process in horizontal pipelines, but this method has limitations on grid size. Liu *et al*. (2023) used the source smoothing method to deal with this problem, so that the particle diameter can be larger than the grid size. However, for two-phase flow problems at high Reynolds number, the calculation accuracy still has high requirements for the grid quality. In comparison, meshless methods can solve these problems effectively.

In this paper, the Lagrangian-Lagrangian coupling method: MPS-DEM method is used to simulate inclined vibration pipelines. At present, some teams have used the MPS-DEM method to simulate flow phenomena and have got results. Harada *et al*. (2019) used the MPS-DEM method to simulate the formation process of ripples on the seabed and used the MPS method to simulate the flow field. In this paper, the control equations for liquid and solid particles, as well as the coupling method between solid and liquid phases are introduced. In addition, the change of flow field under different forms of vibration are analyzed, the numerical simulation results can provide reference for deep-sea mineral transport problems.

2. NUMERICAL METHOD

2.1 Liquid Phase

The control equations of liquid phase based on MPS method are continuity equation and N-S equation, and the equation in Lagrangian form can be written as Eq. 1-3.

$$\frac{\partial}{\partial t}\left(\tilde{\rho}_p\right) + \nabla \cdot \left(\tilde{\rho}_p \vec{u}\right) = 0 \tag{1}$$

$$\frac{D}{Dt}\left(\tilde{\rho}_p \vec{u}\right) = -\nabla p + \varepsilon_p \mu_p \nabla^2 \vec{u} + \tilde{\rho}_p \vec{\mathrm{g}} - \vec{p}_{int} \tag{2}$$

$$\tilde{\rho}_p = \varepsilon_p \, \rho_p \tag{3}$$

Where, ε_p and $\vec{u}$ are local volume fraction and fluid velocity vector respectively. μ_p is dynamic viscosity, $\vec{p}_{int}$ is Volume force caused by momentum exchange between solids and liquids. The MPS method uses kernel functions to discretize the computational domain, and information is also transmitted between particles through kernel functions. In this paper, an improved singularity free kernel function proposed by Zhang *et al*. (2014) is used. Compared with the improved kernel function, when the particle spacing is small, it avoids nonphysical oscillations of pressure and improves the stability of the calculation. The kernel function can be written as Eq .4.

$$W(r) = \begin{cases} \dfrac{r_e}{0.85r + 0.15r_e} - 1 & 0 \le r < r_e \\ 0 & r \ge r_e \end{cases} \tag{4}$$

Where, r_e represents the radius of the particle's scope, and particles with a spacing less than r_e will be determined as neighboring particles.

2.2 Solid Phase

In this paper, the motion equation of the solid phase is calculated by the DEM method. The control equation of the DEM method is Newton's second law, which can be written as Eq. 5-6.

$$m_p \frac{D v_p}{Dt} = \sum_l F_{pq} + m_p \mathrm{g} + F_p^{int} \tag{5}$$

$$I_p \frac{D \omega_p}{Dt} = \sum_l T_{pq} \tag{6}$$

Where, the subscripts p and q represent two solid particles respectively. m_p, I_p, v_p and ω_p represent the mass, moment of inertia, velocity, and angular velocity of solid particles, respectively. F_{pq} and T_{pq} are the mutual force and torque generated by contact between two particles. F_p^{int} is the hydrodynamic vector of liquid acting on solid particles.

For the contact force between two particles, in this paper, the soft sphere model proposed by Cundall *et al*. (1979) is used, as shown in Figure 1.

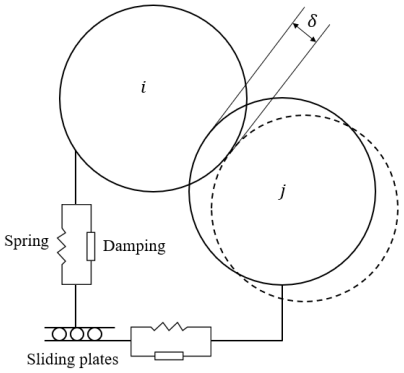

Figure 1. Schematic diagram of soft ball model.

The contact model consists of damping, springs, and sliding plates, which simulate the damping, particle deformation, and frictional force between particles during the collision process respectively. δ is the amount of overlap between two spheres, and the larger δ, the greater the force it is subjected to.

2.3 Interaction Between Two Phases

The interaction between solid and liquid phases is achieved through the transfer of force between the two phases. The force acting on the solid phase is calculated. In this paper, only the relatively large drag and buoyancy forces are considered.

The drag force F_p^d is determined by the local volume fraction of solid particles and the relative velocity with the liquid, it is calculated by the Eq. 7.

$$F_p^d = \frac{\beta_p}{1-\varepsilon_p}\left(u_p - v_p\right)V_p \tag{7}$$

Where, V_p and $v_p$are the volume and velocity of solid particle p respectively. ε_p and u_p are the local volume fraction at the center of the solid particle p and the average velocity of the liquid respectively. β_p is the interface momentum exchange coefficient.

The hydrodynamic vector of liquid acting on solid particles is composed of drag force and buoyancy, it is calculated by Eq. 8.

$$F_p^{int} = \frac{F_p^d}{\varepsilon_p} - V_p\rho_l \mathrm{g} \tag{8}$$

According to the law of conservation of momentum, the reaction force acting on liquid particles from solid particles is calculated by Eq. 9.

$$f_i^{int} = \frac{1}{V_i}\left(F_p^{int}\frac{W_s\left(|r_i - r_p|\right)}{\sum_j W_s\left(|r_j - r_p|\right)}\right) \tag{9}$$

3. NUMERICAL SETUP

3.1 Pipe Model

The pipe model is shown in Figure 2, its length is 4m, and radius is 0.1m. In this paper, the vibration of the pipeline is generated by external excitation. The amplitude distribution along the length of the pipeline can be expressed as Eq. 10.

$$\omega(x) = A\cos\left(\frac{n\pi x}{L}\right)\sin(\omega t) \tag{10}$$

Where, A is the amplitude, ω is the frequency, L is the length of pipeline. Considering that the length of deep-sea mining pipelines can reach several thousand meters, in order to simplify the model, a pipeline with length of 4m was selected for analysis, and it can be approximately assumed that the amplitude distribution is the same along the pipeline length. So, the motion of pipeline can be simplified as a simple harmonic vibration:

$$\omega(x) = A\sin(\omega t) \tag{11}$$

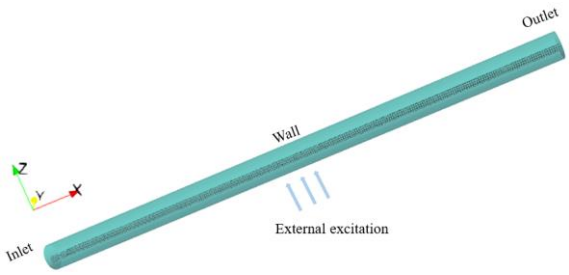

Figure 2. Pipe model.

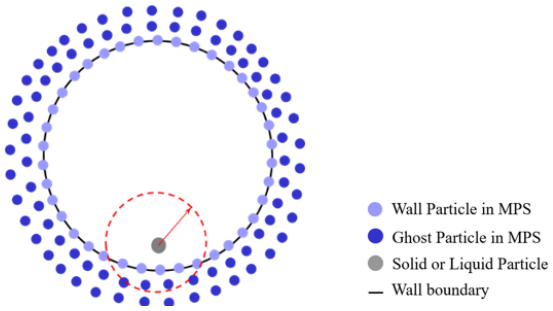

Figure 3. Boundary condition.

Figure 3 shows the boundary conditions, the pipe wall is composed of two types of boundary particles. The Wall particles forms the inner wall of the pipe, and its pressure is calculated by the pressure Poisson equation; the role of ghost particles is to provide support for the wall particles to prevent them from spilling outward.

3.2 Parameters Setup

The parameters of solid and liquid particles are shown in Table 1. The velocity of liquid is 1m/s.
In this paper, three working conditions are set up, as shown in Table 2. The pipeline in Case1 does not vibrate and tilt 40 degrees. In Case2, the direction of vibration is perpendicular to the direction of gravity and along the Y-axis. In Case3, the direction of vibration is the same as that of gravity and along Z-axis.

Table 1. Parameters of Solid and Liquid particles.

Solid phase		Liquid phase	
Parameters	value	Parameters	value
Density (kg/m^3)	2500	Density (kg/m^3)	1025
Diameter (m)	0.015	Kinematic viscosity	1e-6
Young's modulus	100	Particle distance (m)	0.01
Poisson's ratio	0.2	Time step (ms)	0.1
Frictional coefficient	0.2	—	—
Time step (ms)	0.001	—	—

Table 2. Working conditions.

Case	Vibration direction	Period	Amplitude	Angle
Case1	—	—	—	50°
Case2	Along Y-axis	1s	0.08m	50°
Case3	Along Z-axis	1s	0.08m	50°

4. RESULTS

4.1 Influence of Vibration on Pipeline Flow Field

In this section, a comparative analysis is conducted between Case 1 and Case2 to investigate the impact of vibration on the flow field.

4.1.1 Flow State of Solid Particles

Figure 4 shows the flow state of solid particles in pipelines under different cases. As can be seen from the figure, due to the influence of its own gravity, the solid particles accumulate near the inlet of the pipe under both cases, this is because that the kinetic energy the solid particles get from the fluid particles cannot completely offset the influence of gravity, causing some of the solid particles to return to the inlet of the pipe. However, it is obvious that the distribution of solid particles in case1 is more uniform than that in case2, especially in the upper part of the pipe, this indicates that pipe vibration along the Y-axis aggravates the accumulation of solid particles and is more likely to cause pipe blockage. In addition, it also can be seen that the vibration causes the solid particles to move towards the pipe wall. The number of solid particles near the pipe wall in case 2 is significantly more than that in case 1.

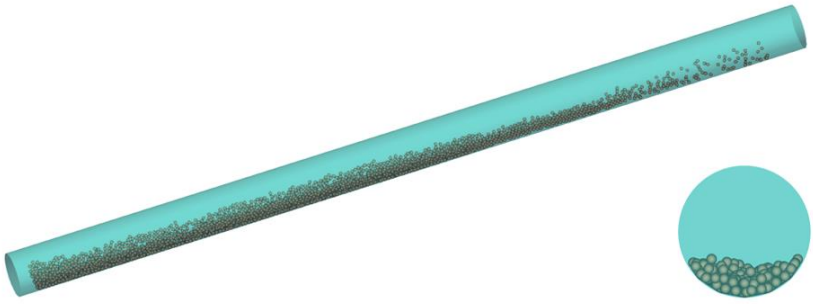

(a) Case1

(b) Case2

Figure 4. Flow state of solid particles.

4.1.2 Volume Fraction

Figure 5 shows the comparison of volume fractions of solid particles at radial distances in different cases.

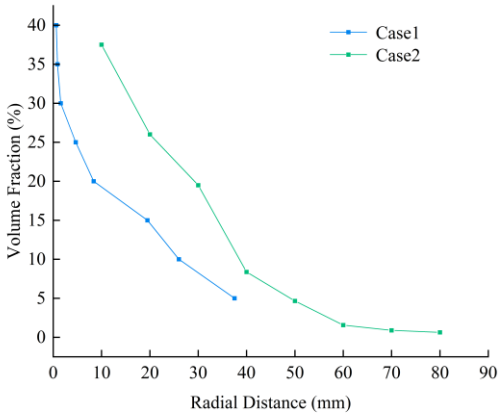

Figure 5. Distribution of volume fraction.

Obviously, the volume fraction distributions of solid particles under case1 and case2 are similar. At the lowest radial distance, i.e., at the bottom of the pipe, the volume fraction is largest. As the radial distance increases, the volume fraction decreases. It is noteworthy that vibration increases the maximum radial distance that solid particles can reach.

4.1.3 Velocity

Figure 6 shows the velocity distribution of solid particles. Overall, the velocity of stationary pipes is greater than that of vibrating pipes. In case1, the maximum velocity of solid particles is located near the center of the pipe. But in case2, vibration causes fluctuations in velocity distribution, and the maximum velocity of solid particles is located near the wall. This may lead to violent friction and collision between the pipe wall and solid particles.

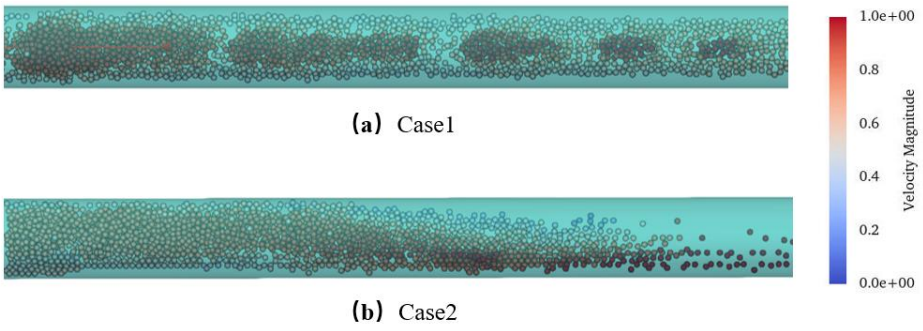

Figure 6. Distribution of velocity.

Figure 7 shows the distribution probability of radial velocity. The probability of radial velocity distribution is approximately the same in two cases, the probability decreases with increasing or decreasing of radial velocity. However, the vibration causes the radial velocity of solid particles increases significantly, solid particles tend to collide with the pipe wall, which increases the loss of kinetic energy and aggravates the particle accumulation.

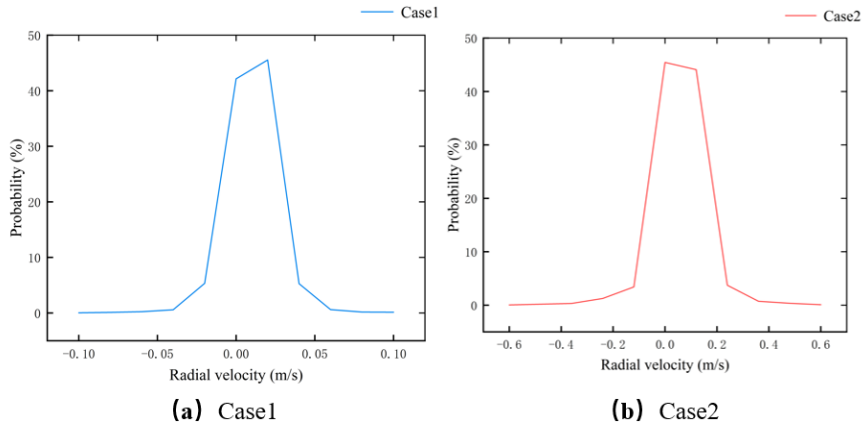

Figure 7. Distribution probability of radial velocity.

4.2 Influence of Vibration Direction on Pipeline Flow Field

In this section, a comparative analysis was conducted on the results of case2 and case3.

4.2.1 Flow State of Solid Particles

Figure 8 shows the flow state of particles with different vibration directions. When the direction of vibration is the same as the direction of gravity, and after the flow field is fully developed, flow of particles will exhibit the characteristics of heterogeneous suspended flow and particles will fill the entire pipeline. In addition, there is still a certain amount of particle accumulation near the pipeline inlet.

(a) Case2

(b) Case3

Figure 8. Flow state of solid particles.

4.2.2 Volume Fraction

Figure 9 shows the volume fraction distribution of solid particles when the vibration direction is different. When the vibration direction is along the Y-axis, the volume fraction continuously decreases with the increase of radial distance, and the distance between the solid particles and the bottom of the pipeline does not exceed 80mm. When the vibration direction is along the Z-axis, the distribution of solid particles becomes more uniform, and the volume fraction first increases and then decreases with the increase of radial distance.

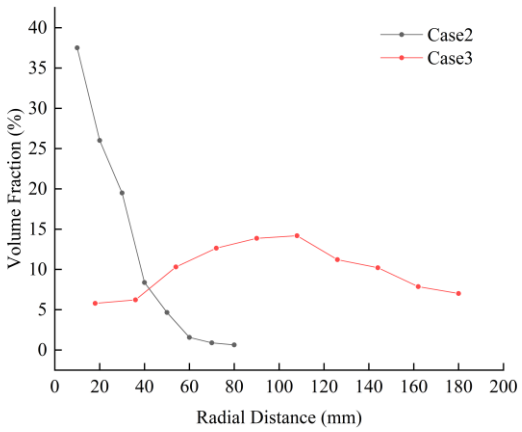

Figure 9. Distribution of volume fraction.

4.2.3 Pressure Loss

Figure 10 shows the pressure loss of liquid when the vibration direction is different. Within a period, pressure fluctuates with time.

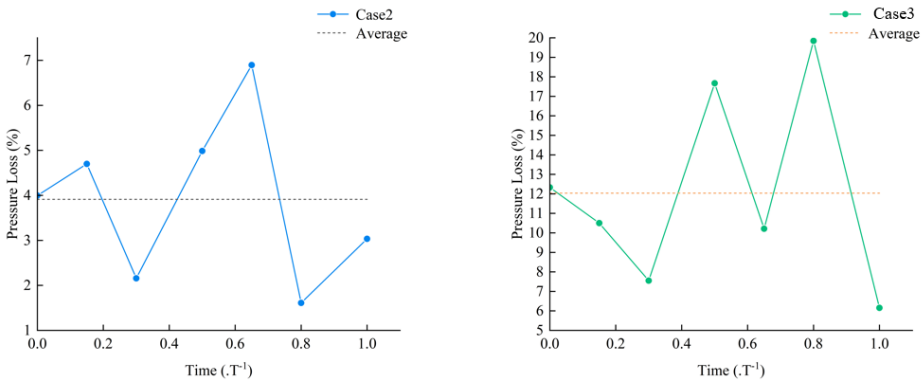

Figure 10. Pressure loss.

The peak and average values of pressure loss in case3 are significantly greater than those in case2, this is because in case3, the distribution of solid particles is more uniform, and the kinetic energy exchange between liquid and solid particles is more frequent, resulting in an increase in pressure loss.

5. CONCLUSIONS

In this paper, by using MPS-DEM method, the influence of vibration and different vibration directions on the flow field is analyzed and obtained the following three results:

(1) The vibration along the Y-axis causes a significant increase in the radial velocity of solid particles, resulting in a loss of kinetic energy and the accumulation of particles at the inlet of the pipeline, which can easily lead to pipeline blockage.

(2) When the vibration direction is perpendicular to the gravity direction, the particle velocity fluctuates, and the maximum velocity is located near the pipe wall.

(3) When the direction of vibration is the same as that of gravity, the volume fraction of particles first increases and then decreases with the increase of radial distance. The distribution of particles in the pipeline becomes uniform, and the exchange of kinetic energy between liquid and solid increases, leading to an increase in pressure loss of the liquid.

ACKNOWLEDGEMENTS

The authors are especially grateful to the Decheng Wan and Fengze Xie for their help in improving the method and MPSDEM-SJTU solver.

REFERENCES

Avi, U and Avi, L. (2018). Flow characteristics of coarse particles in horizontal hydraulic conveying. Powder Technology, 156, 43-51.

OH J W, JUNG J Y, et al. (2015). Gap size effect on the tribological characteristics of the roller for deep-sea mining robot. Marine Georesources & Geotechnology, 35, 120-126.

Hashemi S A, Spelay R B, et al. (2016). Solids velocity fluctuations in concentrated slurries. The Canadian Journal of Chemical Engineering, 94, 1059-1065.

Messa G V, Malavasi S. (2015). Improvements in the numerical prediction of fully-suspended slurry flow in horizontal pipes. Powder Technology, 270, 358-367.

Jafari M, MansoorI Z, Avval M S, et al. (2014). Modeling and numerical investigation of erosion rate for turbulent two-phase gas–solid flow in horizontal pipes. Powder Technology, 267, 362-370.

Martin Robinson, Marco Ramaioli, Stefan Luding. (2014). Fluid–particle flow simulations using two-way-coupled mesoscale SPH-DEM and validation. International Journal of Multiphase Flow, 59, 121-134.

Li Jingjun, Liu Chaoqiu, et al. (2019). Modeling 3D non-Newtonian solid-liquid flows with a free-surface using DEM-MPS. Engineering Analysis with Boundary Elements, 105, 70-77.

Messa G V, Malavasi S, et al. (2014). Numerical prediction of particle distribution of solid-liquid slurries in straight pipes and bends. Engineering Applications of Computational Fluid Mechanics, 8, 356–372.

Avi U, Avi L, et al. (2018). Flow characteristics of coarse particles in horizontal hydraulic conveying. Powder Technology, 326, 302-321.

Liu L, Zhang X T, et al. (2023). Numerical investigation on dynamic performance of vertical hydraulic transport in deep-sea mining. Applied Ocean Research, 130, 103443.

Harada E, Ikari H, et al. (2019). Numerical simulation for swash morpho dynamics by DEM–MPS coupling mode. Coastal Engineering Journal, 61, 2-14.

Zhang Yuxin, Wan Decheng, et al. (2014). Comparative study of MPS method and level-set method for sloshing flows. Journal of Hydrodynamics, 26, 577-585.

Cundall P A, Strack O D, et al. (1979). A discrete numerical model for granular assemblies. Geotechnol, 29, 47-65.